ISSN 2038-5625

Italian Journal of Agrometeorology

Rivista Italiana di Agrometeorologia

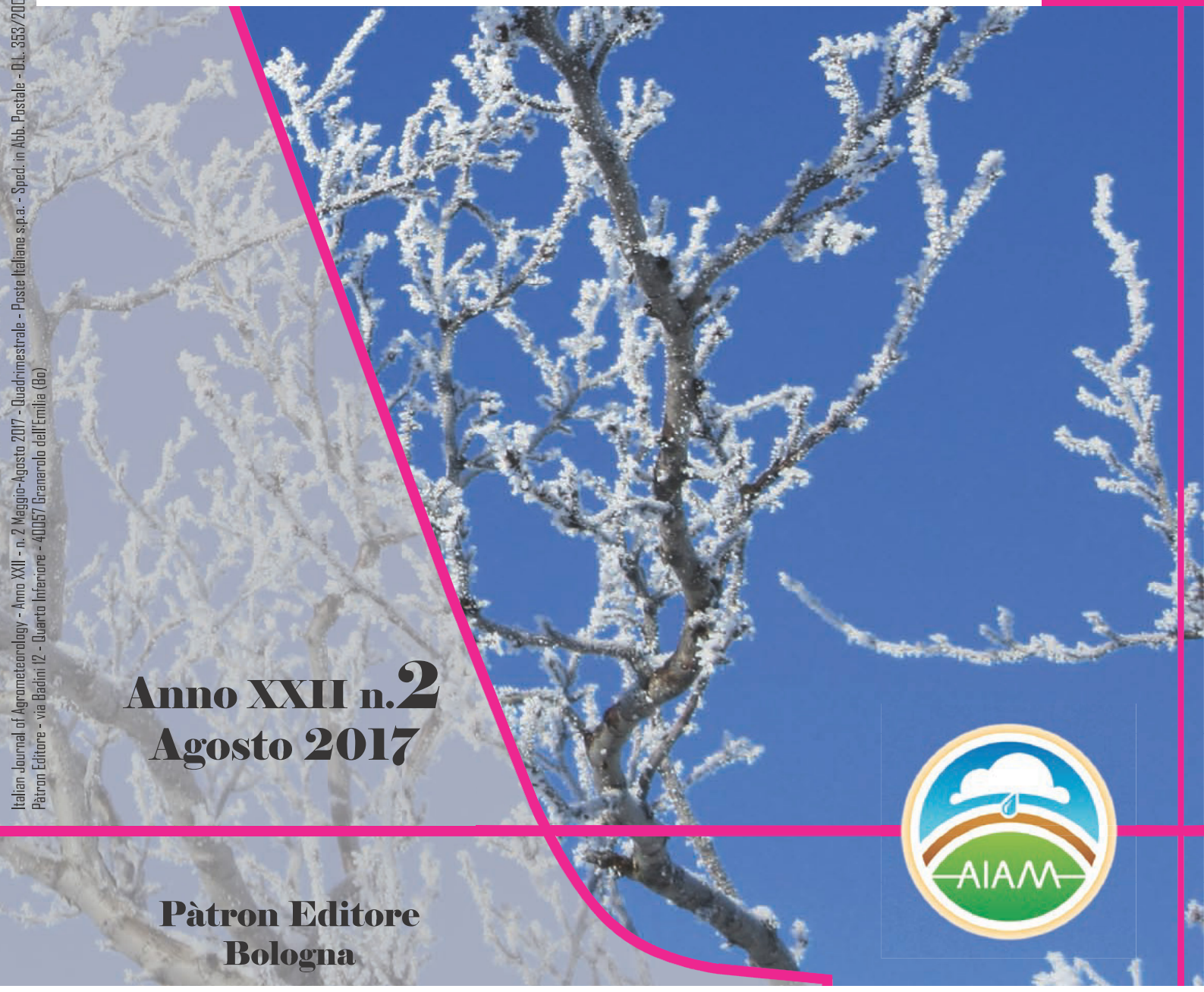

Anno XXII n.2
Agosto 2017

Pàtron Editore
Bologna

Italian Journal of Agrometeorology - Anno XXII - n. 2 Maggio-Agosto 2017 - Quadrimestrale - Poste Italiane s.p.a. - Sped. in Abb. Postale - D.L. 353/2003 (conv. in L. 27/02/2004 n° 46) art. 1, comma 1, CN/BO
Pàtron Editore - via Badini 12 - Quarto Inferiore - 40057 Granarolo dell'Emilia (Bo)

Testing of WRF parameterizations with X-band radar data in a convective rainfall event

Stefania Bolla[1], Marco Branca[2], Claudio Cassardo[1], Silvia Ferrarese[1], Riccardo Notarpietro[2]*

Abstract: *During vegetative season, crops may be damaged by intense rainfall events, such as thunderstorms. In order to limit the risks and to issue thunderstorm warnings, an accurate weather forecast is indispensable. Since the storms occur in limited time and space scales, their forecast is not simple. In this work, the meteorological model WRF was used to simulate convective precipitation associated with an event occurred on 2nd July 2012 in Turin (Italy), and to examine its sensitivity to different schemes of microphysics and clouds parameterization. The precipitation was simulated with 1 km resolution and compared with the observations gathered from a high-resolution X-band radar, operating in the same area during the event.*
Keywords: *WRF model, X-band radar, convective event, precipitation.*

Riassunto: *Durante la stagione della crescita, le coltivazioni possono essere danneggiate da eventi meteorologici intensi, come i temporali. Per limitare i rischi e fornire avvisi sui temporali, è necessaria una accurata previsione meteorologica. Poiché gli eventi temporaleschi avvengono su scale temporali e spaziali limitate, la loro previsione non è semplice. In questo lavoro, il modello meteorologico WRF è stato usato per simulare la precipitazione associata a un evento convettivo avvenuto il 2 luglio 2012 su Torino, e per esaminare la sua sensibilità a diversi schemi di microfisica e di parametrizzazione delle nubi. La precipitazione è stata simulata con la risoluzione di 1 km ed è stata confrontata con quella osservata da un radar in banda X ad alta risoluzione, operativo nella stessa area durante l'evento.*
Parole chiave: *Modello WRF, radar in banda X, evento convettivo, precipitazione.*

1. INTRODUCTION

Heavy storms can be accompanied by strong wind, heavy precipitation, floods, hail and landslides, that can have significant economic, social and environmental impacts. Between heavy storms, the thunderstorms are the product of vigorous convection and they may affect a relatively small area during a relatively short time. One of the most relevant effects of severe thunderstorms is the damage to cultivations and human infrastructures. In particular, severe weather conditions can destroy plants or limit their growth and productivity, with damages that can facilitate subsequent pathologies, with the result of degrading the harvest quality and decreasing its quantity. For agricultural activities, it is therefore of great importance to predict with accuracy thunderstorm development and the amount of precipitation.

Convective precipitation at midlatitudes is hard to forecast in detail, due to the rapid evolution of the meteorological situation (some tenth of minutes) and the small geographical area affected (Fritsch and Carbone, 2004). Actually, thunderstorms are characterized by small spatial and temporal scales, and the degree of predictability depends upon the extension and the duration of coherent rainfall events (Carbone *et al.*, 2002). Therefore, the precise prediction and localization of thunderstorms is a challenge in weather prediction, while the utility of weather forecasts depends upon its accuracy.

Numerical weather prediction models are nowadays largely applied on high-resolution grids, with the ambition to capture phenomena at short temporal and spatial scale, like thunderstorms. However, some physical processes, such as the convection, are active at smaller scales than those resolved by the model grid, and require parameterization schemes to be properly described. Another difficulty in simulating thunderstorms is the presence of complex terrain, where the models could overestimate or underestimate rainfall (Orr and Bechtold, 2009).

The aim of this work is to test the ability of a high-resolution model (the Weather Research & Forecasting model -WRF) in predicting a convective event occurred in the town of Turin (Italy) and its surroundings, composed by rural, urban, hilly and mountainous areas. The region has been selected for three main reasons: I) the presence of large areas devoted to agriculture in the area surrounding Turin city, II) the complexity of the zone, in which there are plain and hilly zones, and the Alps not far away; III) the availability of

* Corresponding author's e-mail: silvia.ferrarese@unito.it
[1] Department of Physics, University of Turin, Italy
[2] Electronics and Telecommunication Department, Polytechnic of Turin, Italy
Submitted 10 November 2015 Accepted 14 December 2016

DOI:10.19199/2017.2.2038-5625.013

a meteorological radar system. As case study of convective event, the episode occurred over Turin, on 2nd July 2012, was analysed.
The results of the simulations were verified by the intercomparison with precipitation data in the same area evaluated from an X-band rain radar. This is a powerful instrument in convective precipitation nowcasting, and it is particularly useful in monitoring heavy rain in complex orography areas (Bertoldo *et al.*, 2012), on a short range. In particular, X-band radars can be used to monitor in detail small basins, towns and valleys prone to flash floods (Gabella *et al.*, 2012). Recently, some X-band radars have been used to estimate the rainfall in some Mediterranean areas for agricultural management (Notarpietro *et al.*, 2013).
The paper is structured as follows. Section 2 introduces the WRF model, Section 3 describes the X-band rain radar, Section 4 presents the case study and Section 5 discusses the results of the simulations. Finally, Sections 6 summarizes the conclusions.

2. WRF MODEL

The WRF model is a high-resolution mesoscale meteorological model, developed since 1990. It has been designed to carry out both operational forecasting and atmospheric research. A detailed description of its equations, physics and dynamics is available in Skamarock *et al.*, (2008).
Regional models are becoming relevant for decision support in agriculture and water management and recently, WRF model applications have been investigated to improve real time choice in agriculture (Müller *et al.*, 2016).
The analysis of past events is useful to understand the performance of the model and to find out the best parameterization settings for different orographic conditions, and in particular meteorological situations. The parameterization is necessary to represent the phenomena taking place on smaller scales than the grid dimension. A great amount of parameterization options are available but, considering rain prediction, the most relevant are: Microphysics and Cumulus Parameterization, which affect cloud and raindrop evolution, influence the cloud formation and the amount of rain (Stensrud, 2007; Zhang *et al.*, 2006). The user can choose among many schemes for both options. The microphysics schemes can be divided in two categories, based on single or double moments. The former predict mixing ratios and resolve one prediction equation for mass (kg/kg) per each species, with particle size distribution being diagnostic; the latter predict mixing ratios and number concentrations (number of raindrops per unit volume as a function of size). Double moment schemes are more complex and, usually, more performing than single moments ones (Hong *et al.*, 2010), because they are more accurate in the representation of particle size distribution, but they are computationally more expensive. In fact, they resolve an additional predictive equation for number concentration (number/kg) for each double-moment species. For this reason, single-moment schemes are often preferred for long simulations.
The sensitivity of cloud microphysics in predicting convective storms and precipitation has already been investigated by many researchers (among others: McCumber *et al.*, 1991; Gilmore *et al.*, 2004; Liu and Moncrieff, 2007; Knebl Lowrey and Yang, 2008, Luo *et al.*, 2010, Shih *et al.*, 2012), trying to understand whether the use of more sophisticated cloud microphysics schemes allows for more precise predictions or not, but definitive results seem not been achieved yet (Rajeevan *et al.*, 2010).
Even bigger uncertainties remain on the role played by cumulus parameterization schemes. The cumulus parameterization schemes are used to predict the collective effects of a great number of convective clouds that may exist within a single grid element of the prediction grid, for grid spacing of 10-20 kilometers (Janjic, 1994; Kain, 2004). The majority of these schemes follow the flux-mass theory, and only one of the available schemes, the Betts-Miller-Janjic, is an adjustment scheme: it adjusts the vertical profiles of temperature and moisture towards a predetermined, post-convection reference profile derived from climatology (Janjic, 1994).
The cumulus schemes are mainly applied at the coarser grid size. In fact, for small grid size (e.g. ≤5 km), the convection could be resolved and therefore the cumulus scheme may no longer be needed (Skamarock *et al.*, 2008). In some heavy convective precipitation events, where high resolution grid have been used, the cumulus schemes have been proven to be unnecessary (Yu and Lee, 2010; Fiori *et al.*, 2014).

3. X-BAND RAIN RADAR

X-band rain radars are characterized by high resolution, small physical size and accessible cost. Having a shorter wavelength (frequencies from 8 to 12 GHz) than the S- or C-band radars, they may observe rain events with high space resolution,

and can be used to monitor very localized heavy storms that cannot be observed by conventional rain/weather radars. On the other hand, they can cover more limited areas and, to overcome this limit, they can be organized in networks (Wang and Chandrasekar, 2010).
The main product is the radar reflectivity (Z), a measure of the power backscattered to the radar from targets existing in any radar resolution cell. If targets are absent, power is not reflected back significantly, and there are no echoes. The reflectivity is also a measure for the total cross section of the particles within the instantaneous measurement volume (the radar resolution cell). From the radar reflectivity, the Rainfall Rate (R) can be evaluated using a power law, such as:

$$Z = a R^b \quad (1)$$

where: a and b are two coefficients reflecting the type of rainfall and the climatological character of a particular location or season (Uijlenhoet, 2001). In case of solid precipitation, typical of cold climates and/or higher latitudes, or even hail, the Z-R relationship (eq. 1) should be applied with different coefficients with respect to the ones normally adopted for rain monitoring.
One of the biggest uncertainties in the evaluation of cumulated rainfall is that the radar cannot see the rain falling on the ground, but can only estimate it from the reflectivity values, at a certain altitude, using the empiric equation Z-R (eq. 1). This relationship depends on parameters that may vary from case to case. The b-coefficient shows no clear dependency on rainfall type (Amitai *et al.*, 2002) and can be regarded as constant over longer time periods, without causing large errors (Steiner and Smith, 2000), while the a-parameter should be continuously adjusted to reflect the short term variations of the vertical profile of reflectivity.
One of the most common method to correct the Z-R relationship is the adjustment of R using gauge measurements of precipitation. The main idea of gauge adjustment is to combine the information taken from these two measurement systems: the information on the spatial distribution of the rain from radar and the high accuracy point measurements from the rain gauges. Obviously, problems connected with gauge-errors and different time and space resolutions of radar and gauges related measurements must also be taken into account. The agreement between radar estimates and gauge point measurements is evaluated using the Bias, defined as the ratio between radar and gauge total precipitation amounts, usually expressed on a logarithmic (decibel) scale (Anagnostou *et al.*, 1998, Gouden-hoofdt and Delobbe, 2009).
Radar estimates of rainfall are affected by uncertainties, which are both systematic and random in nature. A complete discussion of these errors is reported in the review paper of Villarini and Krajewski (2010). Empirical models have been developed to represent the uncertainties in the form of ensamble (Villarini *et al.*, 2014), for a review: Mandapaka and Germann (2010).

3.1 X-band radar main features

In this work, data from the Polytechnic of Turin X-band radar were used. This is a pulsed radar, placed on the roof of the university building, at latitude 45.063° N, longitude 7.660°E, and at 25 meters above ground level (at about 249 m a.s.l.). It covers a circular area of 30 km radius, including the city of Turin, some nearby towns (Fig. 1), several cultivated and grassland areas. The radar beam axis at a fixed 1° elevation reaches an altitude of about 550 m and the beam width is 3.6°. The resolution of the reflectivity data, covering the overall area, is 60 x 60 m^2. The technical features of the radar are reported in Tab. 1 (Gabella *et al.*, 2012; Turso *et al.*, 2013). The data are acquired in the polar coordinate system, and then converted into the Cartesian one, where each pixel contains the spatial average of all the values of the polar pixels included in the Cartesian one. The coefficients a and b in eq. (1) have been set to 300 and 1.6, respectively, as estimated in a previous study in the same area (Gabella and Notarpietro, 2004).The interferences

TRANSMITTER	
Peak power	10 kW
Pulse length	400 ns
Transmitted frequency	(9410 ± 30) MHz
PRF	800 Hz
Modulator	Solid state
RECEIVER	
Receiver type	Logarithmic, solid state
Dynamic range	From 0 to 10 dBm
Intermediate frequency	60 MHz
Receiver filter bandwidth	(20 ± 2) MHz
OTHER SPECIFICATION SHEET	
Front end	Microwave integrated circuit
Noise figure	< 3.5 dB
Duplexer	Ferrite circulator with state solid diode limiter
Antenna rotation speed	(22 ± 2) r.p.m.
Power	24 Vdc

Tab. 1 - Technical characteristics of the X-band radar.
Tab. 1 - Caratteristiche tecniche del radar in banda X.

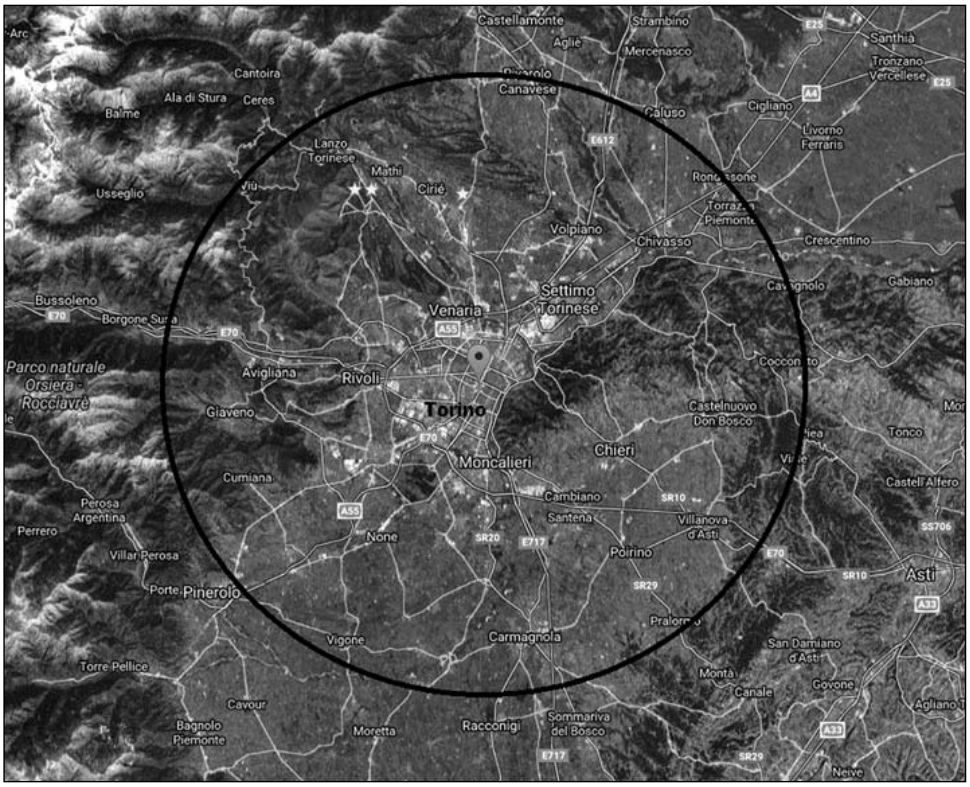

Fig. 1 - Area covered by the X-band radar.
Fig. 1 - Area del radar in banda X.

with other active radars and the terrain echoes or clutter can cause errors in the radar-data. To reduce these anomalous data, an anti-bang filter and a series of anti-clutter filters are applied, as described in Bertoldo *et al.* (2012).

The radar used in this work, being placed in a lower position with respect to the neighbor hills and mountains, is subject to beam occultation. In fact, observing an image coming from a data system, we could see dark or shadowed areas of regular form where the radar cannot see any event, such as in Fig. 2. This phenomenon is caused by the presence of urban buildings (urban clutter) or orographic obstacles (ground clutter), which interfere with the radar-beam, causing an occultation of the area behind it. The occultation can be total or partial; in the first case, there is no backscattered signal at all, while in the latter there is a great attenuation of the signal.

Thus, due to the presence of hills and buildings in the area covered by the radar, a portion of the acquired data is not reliable and therefore has been excluded from the analysis. To identify the useful area, in the present work, the radar cumulated precipitation maps during three months (May, June and July 2012) were considered. Only the zones where the measured radar cumulated precipitation was higher than a fixed threshold were considered as unaffected by beam occultation. The threshold is case-dependent: in the studied area and during the three mentioned months some tests with different values have been performed, and the value of 15 mm has been identified as the best choice allowing to distinguish between areas affected or not by beam occultation.

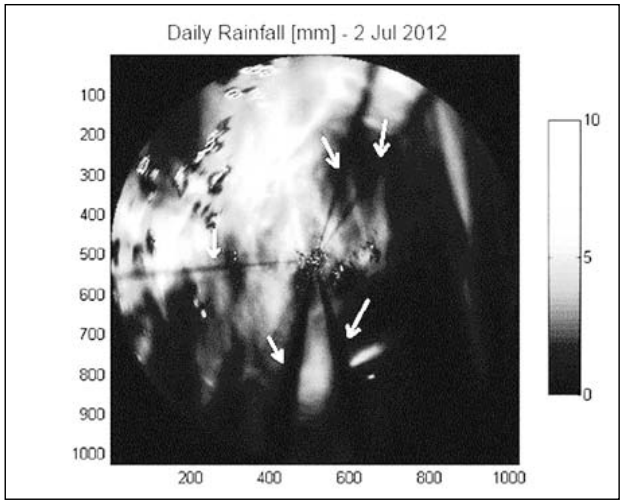

Fig. 2 - Beam occultation occurred during the data acquisition on 2nd July 2012. The white arrows indicate some dark areas evidencing this problem.
Fig. 2 - Occultazione del fascio durante l'acquisizione dei dati il 2 luglio 2012. Le frecce bianche indicano alcune aree scure evidenziando questo problema.

In the selected areas, three raingauges from Weather Underground network were active during the event. Their geographical coordinates (latitude and longitude) are: 45.236°N, 7.507°E; 45.232°N, 7.640°E; 45.236°N, 7.527°E. The evaluated preci-pitation by the radar and that measured by the raingauges has been compared using a contingency table, as described in Section 6. The comparison has shown a good agreement between the point data from raingauges and the radar data.

4. CASE STUDY

The analyzed case-study is a heavy rainfall event occurred on 2nd July 2012 in Piedmont region (NW Italy). The rainfall occurred during two distinct severe thunderstorms, one in the earlier hours of the morning and the other one in the afternoon. The first event was originated by the progressive rotation of wind direction at the various levels, from ESE near the surface to SSE at 950 and 850 hPa, SE at 700 hPa, and S at 500 hPa. The resulting convergence, amplified by the orographic Alpine reliefs, represented the trigger mechanism that initiated the convection at the lower levels, furtherly amplified by the instability present above the boundary layer. Regarding the afternoon rainfall, the meteorological factor was the irruption of cold air on Piedmont region, caused by a temporary pulsation of one of the secondary branch of a deep 500 hPa through located on Atlantic ocean, extended on France and with its axis tilted from NW to SE. The cold and dry air associated to this through crossed the NW Alps in the early afternoon of 2nd July, first at 850 hPa (Fig. 3) and some hours later also at the soil level, then pushing vertically the preexisting deep layer of warm and humid air, created by southern winds present in the whole northern Italy at all levels (and also over Piedmont till the morning). The flow generated also a temporary minimum over Piedmont region during the afternoon. This large gradient of temperature and moisture over the prealpine regions increased the instability already present on Po valley. The CAPE values at the radiosounding station of

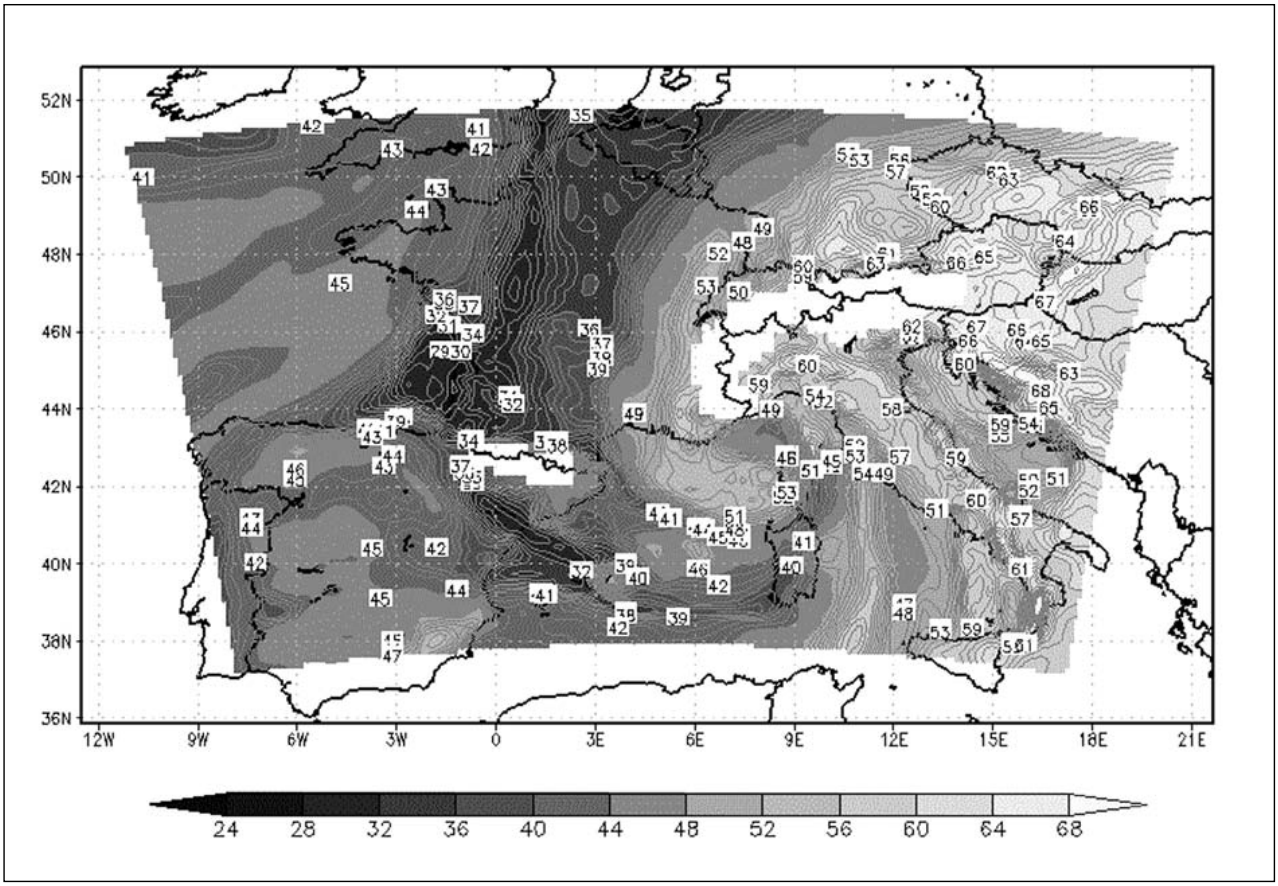

Fig. 3 - Equivalent potential temperature in the greater WRF domain at 850 hPa, 2nd July 2012 at 12:00 UTC.
Fig. 3 - Temperatura potenziale equivalente nel grigliato più esteso del modello WRF a 850 hPa, 2 luglio 2012 alle ore 12:00 UTC.

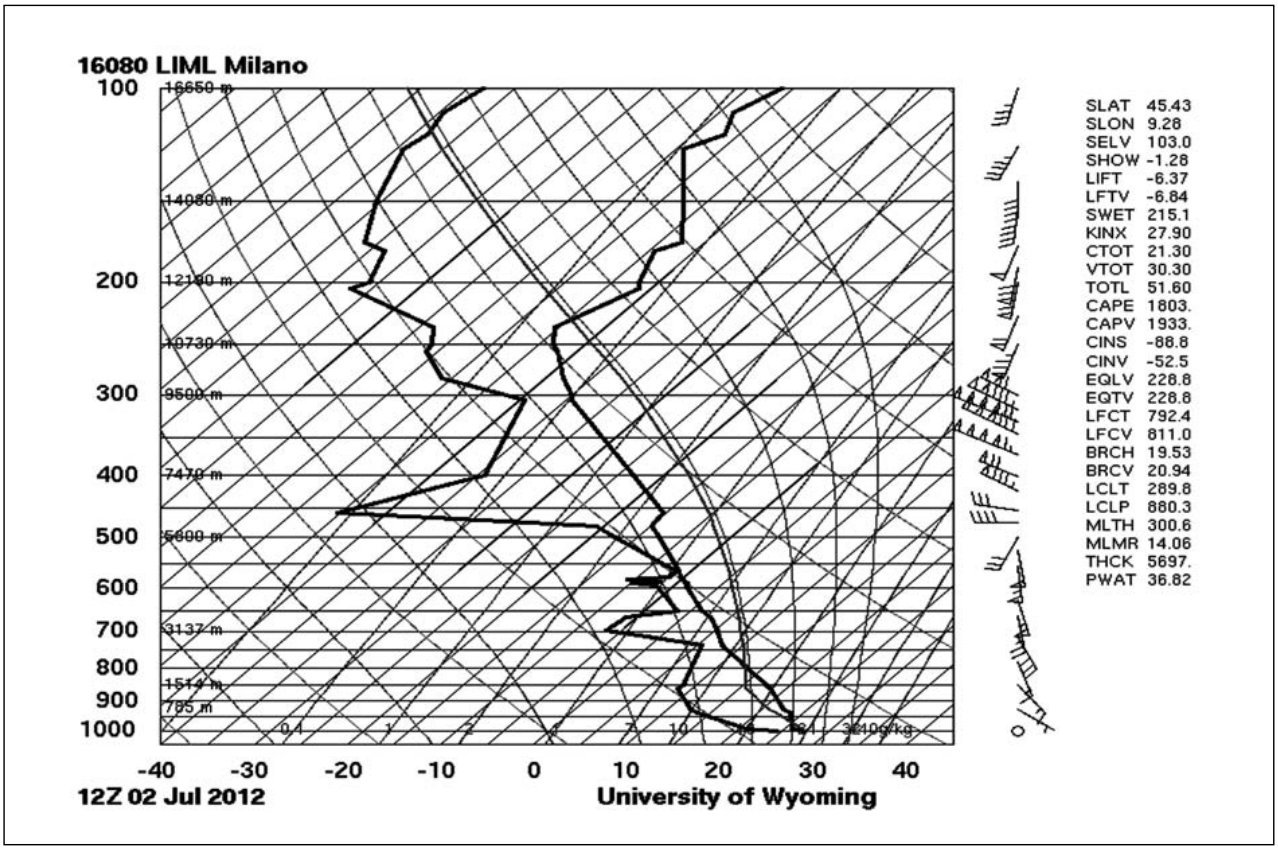

Fig. 4 - The radiosounding at Milano station, Italy, 2nd July 2012 at 12:00 UTC (source: weather.uwyo.edu).
Fig. 4 - Il radiosondaggio della stazione di Milano, Italia, 2 luglio 2012 alle ore 12:00 UTC (fonte: weather.uwyo.edu).

Milano (Fig. 4), the only available in the area at that time, were already large during midnight – up to 800 m^2s^{-2}, and grew up to 1800 m^2s^{-2} in the afternoon. This irruption gave origin to a first line of diffuse thunderstorms that crossed the Piedmont region, due to the instability and the contrast between the two air masses. Other thunderstorms continued to be generated also in the late morning and afternoon, when cold air irrupted also at the soil level, destabilizing the air column. Only in the evening, when the new air mass took possess of the whole region, the phenomena ceased.

This dynamics helps to understand why the first rainfall on Turin city was recorded in the earlier hours of the morning (from midnight to 4 a.m.), and then other episodes occurred between late morning and the afternoon (from 11 a.m. to 6 p.m.); all hours here are in UTC time. Several raingauges were active in the area of Torino and it surroundings, but only three of them were located in the radar not-cluttered zone. In the early hours of the morning they measured moderate values of cumulated precipitation (20 mm, 9 mm and 18 mm) and more intense quantities in the afternoon (15 mm, 59 mm and 29 mm).

5. SIMULATIONS

The event of 2nd July 2012 over Turin town and its surroundings was simulated by the WRF model, version 3.6. Ten simulations were executed in order to evaluate the sensibility of cumulus and microphysical parameterizations. The other parametrization schemes, available in WRF, remained unchanged. The list of the common schemes in all simulations is reported in Tab. 2.

Spatial and temporal domains and initial and boundary conditions were unchanged in the ten tests. All simulations were run for three days, from

Physics	Scheme
Longwave radiation	RRTM
Shortwave radiation	Dudhia
Surface Layer	MM5 similarity model
Land Surface	Noah
Planet Boundary Layer	YSU

Tab. 2 - Common schemes in all simulations.
Tab 2. - Schemi comuni a tutte le simulazioni.

30th June 2012 at 00 :00 UTC, to 3rd July 2012 at 00:00 UTC. Usually the first simulated 12-24 h are not used because the meteorological model must adjust the fields over the orography and it needs time for the formation of cloud and precipitation, because it starts with zero clouds and precipitation particles. In the present paper, the studied event occurred on 2nd July 2012, but it was part of an intense perturbation that took origin in the NW Europe one day before. Therefore, the simulations started on 30th June 2012, 24 h before the perturbation arrival on the continent and 48 h before the beginning of the precipitation event over the Piedmont region.
As for the spatial domains, starting from a coarser grid of low resolution (27 km), three nests with finer resolutions (9, 3 and 1 km, respectively) were created and centered over the study area (Fig. 5). Details of temporal and spatial domains setting can be found in Tab. 3.
To generate the initial data and boundary con-ditions for the coarser grid of the simulations, meteorological data from the ECMWF (European Centre for Medium-Range Weather Forecast) were downloaded. The analyses every 6 hours with 0.5°x0.5° resolution in longitude and latitude respectively (which means about 40 km along x direction and 55 km along y direction, at Turin position) were used.

	Resolution [km]	Grid Points (x,y)	Integration time-step [s]	Output time-step [s]
1st grid	27	85x60	81	10800
2nd grid	9	79x58	27	3600
3rd grid	3	85x73	9	3600
4th grid	1	109x97	3	3600

Tab. 3 - WRF temporal and spatial domain settings.
Tab 3 - Impostazioni temporali e spaziali dei dominii WRF.

Five simulations (1 – 5 in Tab. 4) were devoted to test some of the available cumulus parameterization schemes. Among the cumulus schemes available on WRF, the schemes which take in account both shallow and deep convection, were tested: Kain-Fritsch (Kain, 2004), Betts-Miller-Janjic (Janjic, 1994; Janjic, 2000), SAS (Pan and Wu, 1995), Tiedtke (Tiedtke, 1989; Zhang *et al.*, 2011) and NSAS (Han and Pan, 2011). In all simulations, the cumulus parameterizations were applied to both first and second domains, whose resolution was lower or equal than 9 km, whereas in the third and fourth domains (with resolutions of 3 and 1 km, respectively) the cumulus parameterization was not applied like suggested in the WRF technical note (Skamarock *et al.*, 2008). Furthermore, an additional test was performed (simulation 6) with deep convection explicitly resolved (no cumulus

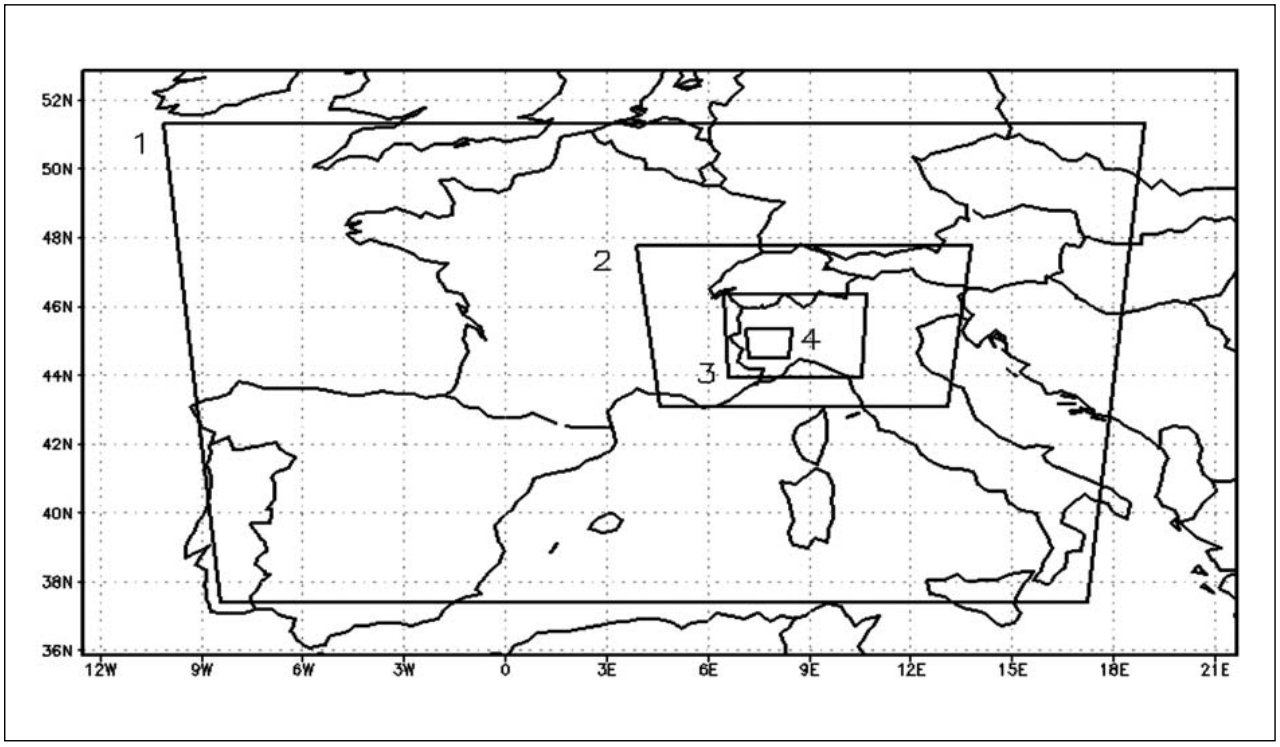

Fig. 5 - Nested grids.
Fig. 5 - I grigliati innestati.

parameterization scheme activated in all four domains) to explore the model performance without the cumulus scheme. Regarding the microphysical parameterization selection, actually WRF considers several schemes. To limit the simulation number, a complex and complete scheme has been chosen: a double-moment scheme with more mixing-ratios. This method is not exhaustive, but it permits to test the model schemes. For the experiments, the Morrison double-moment scheme was selected (Morrison and Gettelman, 2008); this is a two-double moments bulk scheme that considers six mixing ratios (vapor, rain, snow, cloud ice, cloud water and graupel) and four number concentrations (ice, snow, rain and graupel).

A second group of simulations (1 and 7–10) aimed to test the impact of microphysics scheme in rain prediction. A single moment (WSM6) and four different double-moment schemes (Morrison, WDM6, Milbrandt, NSSL) were used (Tab. 4). The single moment WSM6 scheme (Hong and Lim, 2006) is widely used in WRF community, especially for operative applications, because of its computational efficiency. However, due to the difficulty of the convective rain prediction and the short-time covered by the studied precipitation, double-moment models were chosen for the other four simulations (1 and 8-10). WDM6 scheme (Lim and Hong, 2010) is similar to the WSM6, but it also predicts the prognostic number concentration of rain and cloud water and cloud condensation nuclei. Milbrandt scheme (Milbrandt and Yau, 2005) is a double-moment mixed-phase scheme that predicts cloud, rains, ice, snow, graupel and hail mixing ratios. It also predicts the number concentrations for every species. NSSL (Mansell *et al.*, 2010) is a double-moment scheme for water vapor, cloud droplets, rain drops, ice crystals, snow, graupel and hail. In these four simulations, the Kain-Fritsch cumulus scheme was fixed.

Simulation	Cumulus scheme	Microphysics scheme
1	Kain-Fritsch	Morrison
2	Betts-Miller-Janjic	Morrison
3	SAS	Morrison
4	Tiedtke	Morrison
5	NSAS	Morrison
6	Explicit	Morrison
7	Kain-Fritsch	WSM6
8	Kain-Fritsch	WDM6
9	Kain-Fritsch	Milbrandt
10	Kain-Fritsch	NSSL

Tab. 4 - Cumulus and microphysics schemes in the 10 simulations.
Tab 4 - Schemi per cumuli e microfisica nelle 10 simulazioni.

6. RESULTS

The comparison between observation and forecast is usually performed building a contingency table (Tab. 5) for dichotomous verification (Wilks, 1995). In the present work three statistical indexes were used: Accuracy, fractional Bias and Heidke Skill Score. The Accuracy (*acc*) is the averaged degree of correspondence between individual pairs of forecasts and observations

$$acc = \frac{hits + correct\ negative}{total}$$

where

$$total = hits + correct\ negative + misses + false\ alarms$$

The accuracy index can vary from 0 to 1, where 1 represents the perfect match between forecast and observation.

The fractional Bias is defined as the degree of correspondence between the total number of forecasted events and the total number of observed events:

$$Bias = \frac{hits + false\ alarms}{hits + misses}$$

The Bias can vary from 0 to infinity, where 1 means a perfect score, and other values can evidence over- or under-estimations.

The Heidke Skill Score (HSS) measures the ability of the model to make correct predictions, after eliminating the correct prediction due to chance:

$$HSS = \frac{(hits + correct\ negative) - expected\ correct}{total - expected\ correct}$$

where:

$$expected\ correct = \frac{1}{total}[(hits + misses)(hits + false\ alarms) + (correct\ negatives + misses)(correct\ negatives + false\ alarms)]$$

HSS can vary from -1 to 1, where 1 stands for a 100% of correct predictions.

Firstly, the comparison between the radar precipitation data and the measured one by three raingauges has been performed. In this test, the data from raingauges are the observations whereas

	Observed yes	Observed no
Forecast yes	hits	false alarms
Forecast no	misses	correct negatives

Tab. 5 - Contingency table. Hits: number of pixels with forecasted and occurred rainfall; misses: number of pixels where rainfall was not forecasted but observe; false alarm: number of pixels in which rainfall was forecasted but not observed; correct negative: number of pixels in which rain was not forecasted and not observed.
Tab. 5 - Tabella di contingenza. Hits: numero di pixels con pioggia prevista ed avvenuta; misses: numero di pixels dove la pioggia non è stata prevista ma è stata osservata; false alarms: numero di pixels nei quali la pioggia è stata prevista ma non osservata; correct negatives: numero di pixels nei quali la pioggia non è stata prevista e non è stata osservata.

the radar data are the forecasts. The computed accuracy is 0.86, the bias is 1.00 and the HSS is 0.72. These values confirm the goodness of radar data and authorize their use in the analysis of the simulation results.
Secondly, radar-derived precipitation and model-simulated one has been compared. The comparison is possible applying several techniques (Rossa *et al.*, 2005). Here, the verification approach with contingency tables was used, where forecast stand for simulation result and observation for radar data. The method involved the couples of observed and simulated rainfall values over each grid cell in the same area and at the same time intervals (Paolella *et al.*, 2011). As the radar pixels were smaller than the model grid size (60 x 60 m^2 versus 1 x 1 km^2), the radar observations were averaged, lowering their resolution to model resolution. At every radar data pixel was assigned a new coordinate value corresponding to the WFR cell, whose center is nearer to the radar pixel center. Then, the average of all the radar rain data contained in a single WRF cell was calculated. The comparison has involved the spatial area with higher simulation resolution and the temporal interval from 2nd July at 00:00 UTC to 3rd July at 00:00 UTC.
Tab. 6 shows the computed indices for all simulations. In this table, the simulations could be grouped in two subsets:

1) Cumulus parameterization study (simulations 1– 6).
   The simulation results are similar for all schemes. The simulation showing maximum accuracy and HSS indices (respectively 0.70 and 0.40) is the simulation number 6, followed by the number 2 (0.69 and 0.38). As regards Bias index, the best value is obtain by simulation 3, but also the other simulations have comparable values. In conclusion, slightly better performances are shown by simulations 2 and 6, therefore using Betts-Miller-Janjic scheme or the explicit parameterization, respectively. Therefore, the use of a cumulus parameterization scheme did not sensibly influence the results, probably because the microphysics double moment scheme (Morrison) is advanced enough to predict the convective rain.
2) Microphysics study (simulations 1 and 7-10).
   The indices clearly show that the single-moment scheme WSM6 is less performing than the others; this result proves that convective rain is better predicted using complex double-moment schemes. Among the double moment schemes tested, WDM6 show the worst skills, giving results similar to the WSM6 scheme, but with a larger bias. In this set of simulations the best microphysics scheme seems to be the Morrison double moment scheme (simulation 1), with a 0.66 of accuracy, 0.94 of Bias and a 0.32 of HSS, followed by the NSSL scheme, with less performing values. Therefore, the choice of microphysics is a critical option for the simulation performance.

Simulation	acc	Bias	HSS
1 Kain-Fritsch - Morrison	0.66	0.94	0.32
2 Betts-Miller-Janjic - Morrison	0.69	0.99	0.38
3 SAS - Morrison	0.68	1.00	0.36
4 Tiedtke - Morrison	0.65	0.91	0.30
5 NSAS - Morrison	0.65	1.08	0.30
6 Explicit - Morrison	0.70	1.03	0.40
7 Kain-Fritsch - WSM6	0.56	0.38	0.09
8 Kain-Fritsch - WDM6	0.58	0.69	0.14
9 Kain-Fritsch - Milbrandt	0.61	0.60	0.20
10 Kain-Fritsch - NSSL	0.61	0.86	0.20

Tab. 6 - Comparison between simulated and observed precipitation.
Tab. 6 - Confronto tra precipitazione simulata ed osservata.

7. CONCLUSIONS

Convective events are particularly hard to predict, due to the typical short duration of the showers and to the turbulent nature of the events themselves. Nevertheless, the forecast of this kind of events is very important in the agricultural management, especially in zones like Piedmont region, in which several cultivations are present. The possibility to know which kind of phenomenon could affect some areas may be helpful for farmers to plan their agricultural practices, including also the fight against infections and diseases, frequently affected by humidity and rainfall.

Mesoscale models are now a precious tool to forecast convective rain on crops and to support the decision systems. In this work, the WRF model sensitivity to different parameterizations was studied, allowing to identify the best combination of schemes. The case-study analyzed was a convective rainfall event that took place on 2nd July 2012 in the NW Italy, and was formed by a shorter morning rain event (from 0 to 4 a.m.) and a longer afternoon event (from 11 a.m. to 6 p.m.). Despite the choice and analysis of one specific case study, the authors are confident that this event is widely representative of several thunderstorm events in Piedmont region.

Ten WRF simulations were run, in order to test different cumulus and microphysics parameterization schemes. For each test, the simulated precipitation has been compared with the data derived from a high resolution X-band rain radar located in Turin city.

Among the two parameters tested, the cumulus and the microphysics parameterizations, the most relevant in convective rain prediction is the second one. In fact, the cumulus parameterization schemes tested have little influence on the ability of the WRF model to predict the rain event: similar results were obtained using the five cumulus schemes and the explicit one. In particular, the two best results were computed using the Betts-Miller-Janjic scheme or without the use of any scheme at all. As regards the microphysical parametrization, one single-moment scheme and various double-moment models were tested. As expected, the single-moment scheme turned out to be less performing than the others. In this case-study, the higher accuracy in rain prediction was obtained using the Morrison and the NSSL schemes. Besides, the double-moment appears to be complex enough to predict a convective rain without the application of any cumulus parameterization scheme.

In conclusion, in this convective case-study, the use of a complex microphysics scheme, coupled with explicit parameterization (without cumulus parameterization scheme), seems to be a preferable choice in order to allow a sufficiently detailed and performing prediction. Such result could have profound implications for agricultural areas intensely cultivated, as well as for the protection of civil infrastructures.

ACKNOWLEDGMENTS

The authors thank Weather Underground Inc. for the availability of precipitation data.

REFERENCES

Amitai E., Wolff D. B., Marks D. A., Silberstein D. S., 2002. Radar rainfall estimation: lessons learned from the NASA/TRMM validation program. In: Proceedings of ERAD 2002, ERAD publication series, 1: 255-260.

Anagnostou E.-N, Krajewski W.-F., 1998. Real-time radar rainfall estimation. Part I: algorithm formulation. Journal of Atmospheric and oceanic Technology, 16: 189-197.

Bertoldo S., Lucianaz C., Rorato O., Allegretti M., Prato A., Perona G., 2012. An operative X-band mini-radar network to monitor rainfall events with high time and space resolution. ETASR – Engineering, Technology & Applied Science Research, 2: 246-250.

Carbone R. E., Tuttle J. D., Ahijevych D. A., Trier S. B., 2002. Inferences of Predictability Associated with Warm Season Precipitation Episodes. Journal of the Atmospheric Science, 59: 2033-2056.

Fiori E., Comellas A., Molini L., Rebora N., Siccardi F., Gochis D.J., Tanelli S., Parodi A., 2014. Analysis and hindcast simulations of an extreme rainfall event in the Mediterranean area: The Genoa 2011 case. Atmospheric Resources, 138: 13-29.

Fritsch J. M., Carbone R. E., 2004. Improving quantitative precipitation forecasts in the warm season: A USWRP research and development strategy. Bulletin of the American Meteorological Society, 85: 955-965.

Gabella M., Notarpietro R., 2004. Improving operational measurement of precipitation using radar in mountainous terrain-Part I: methods. IEEE Geoscience and Remote Sensing Letters, 1: 78-83, doi: 10.1109/LGRS.2003.822311.

Gabella M., Notarpietro R., Bertoldo S., Prato A., Lucianaz C., Rorato O., Allegretti M., Perona

G., 2012. A Network of Portable, Low-Cost, X-Band Radars, Doppler Radar Observations - Weather Radar, Wind Profiler, Ionospheric Radar, and Other Advanced Applications, In: Bech J. (ed.) InTech, Croatia, ISBN: 978-953-51-0496-4: 175-202.

Gilmore M. S., Straka S. M., Rasmussen, E. N., 2004. Precipitation and evolution sensitivity in simulated deep convective storms: comparisons between liquid-only and simple ice and liquid phase microphysics. Monthly Weather Review, 132: 1897-1916.

Goudenhoofdt E., Delobbe L., 2009. Evaluation of radar-gauge merging methods for quantitative precipitation estimates. Hydrology and Earth System Science, 13: 195-203

Han J., Pan H.-L., 2011. Revision of Convection and Vertical Diffusion Schemes in the NCEP Global Forecast System. Weather and Forecasting, 26: 520-533.

Hong S.-Y., Lim J.-O. J., 2006. The WRF single-moment 6-class microphysics scheme (WSM6). Journal of the Korean Meteorological Society, 42: 129-151.

Hong S.-Y., Lim K.-S. S., Lee Y.-H., Ha J.-C., Kim H.-W., Ham S.-J., Dudhia J., 2010. Evaluation of the WRF Double-Moment 6-Class Microphysics Scheme for Precipitating Convection. Advances in Meteorology, 2010: 10 pages.

Janjić Z. I., 1994. The step-mountain eta coordinate model. Further developments of the convection, viscous sublayer and turbulence closure schemes. Monthly Weather Review, 122: 927-945.

Janjić Z. I., 2000. Comments on "Development and evaluation of a convection scheme for use in climate models.". Journal of the Atmospheric Science, 57: 3686-3686.

Kain J. S., 2004. The Kain–Fritsch convective parameterization: An update. Journal of Applied Meteorology, 43: 170-181.

Knebl Lowrey M. R., Yang Z.-L., 2008. Assessing the capability of a regional-scale weather model to simulate extreme precipitation patterns and flooding in central Texas. Weather and Forecasting, 23: 1102-1126.

Liu C., Moncrieff M. W., 2007. Sensitivity of cloud-resolving simulations of warm-season convection to cloud microphysics parameterizations. Monthly Weather Review, 135: 2854-2868.

Lim K.-S. S, Hong S.-Y., 2010, Development of an effective double-moment cloud microphysics scheme with prognostic cloud condensation nuclei (CCN) for weather and climate models. Monthly Weather Review 138: 1587-1612.

Luo Y., Wang Y., Wang H., Zheng Y., Morrison H., 2010. Modeling convective-stratiform precipitation processes on a Mei-Yu front with the Weather Research and Forecasting model: Comparison with observations and sensitivity to cloud microphysics parameterizations. Journal of Geophysical Research, 115, D18117, doi:10.1029/2010JD013873.

Mandapaka P. V., Germann U., 2010. Radar-Rainfall error models and ensemble generators. Rainfall: State of the Science, Geophysical Monograph Series 191:247-264.

Mansell E. R., Ziegler C. L., Bruning E. C., 2010. Simulated electrification of a small thunderstorm with two-moment bulk microphysics. Journal of the Atmospheric Science, 67: 171-194.

McCumber M., Tao W.-K., Simpson J., Penc R., Soong S.-T., 1991. Comparison of Ice-Phase Microphysical Parameterization Schemes Using Numerical Simulations of Tropical Convection. Journal of Applied Meteorology, 30: 985-1004.

Milbrandt J.A., Yau M. K., 2005. A multimoment bulk microphysics parameterization. Part II: A proposed three-moments closure and scheme description. Journal of the Atmospheric Sciences, 62: 3081-3065.

Morrison H., Gettelman A., 2008. A new two-moment bulk stratiform cloud microphysics scheme in the community atmosphere model, version 3 (CAM3). Part I: Description and numerical tests. Journal of Climate, 21: 3642-3659.

Müller O., Lovino M., Berbery E., 2016. Evaluation of WRF model forecasts and their use for hydroclimate monitoring over southern South America. Weather and Forecasting. doi:10.1175/WAF-D-15-0130.1, 31: 1001-1017.

Notarpietro R., Branca M., Morin E., Lokshin A., Gabella M., De Vita P., Basso B., Bonfil D., Bertoldo S., Shah S., Lucianaz C., Rorato O., 2013, Towards sustainable agricultural management using highresolution X-band radar precipitation estimates. Electromagnetics in Advanced Applications (ICEAA), 2013 International Conference on Electromagnetics in Advanced Applications, Torino, pp. 915-918, doi: 10.1109/ICEAA.2013.6632373.

Orr A., Bechtold P., 2009. Improvement in

the capturing of short-range warm season orographic precipitation in the ECMWF model. Meteorology and Atmospheric Physiscs, 103: 15-23.

Paolella S., Prato A., Turso S., Notarpietro R., Bertoldo S., Cucca M., Gabella M., Perona G., Ferrarese S., Richiardone R., 2011. Identification, tracking, validation and forecast of local high resolution precipitation patterns observed through X-band micro radars. Electromagnetics in Advanced Applications (ICEAA), 2011 International Conference on Electromagnetics in Advanced Applications, Torino, pp. 1436-1439, doi: 10.1109/ICEAA.2011.6046290.

Pan H.L., Wu W.S., 1995. Implementing a mass flux convection parameterization package for the NMC Medium-Range Forecast Model. Office note 409. National Meteorological Center.

Rajeevan M., Kesarkar A., Thampi S. B., Rao T.N., Radhakrishna B., Rajasekhar M., 2010. Sensitivity of WRF cloud microphysics to simulations of a severe thunderstorm event over Southeast India. Annales Geophysicae, 28: 603-619.

Rossa A., Bruen M., Frhwald D., Macpherson B., Holleman I., Michelson D., Michaelides S., 2005. Use of Radar Observations in Hydrological and NWP Models. Final Report of COST 717, EUR 21954, Brussels: 286 pages.

Shih D.-S., Liau J.-M., Yeh G.-T., 2012. Model assessments of precipitation with a unified regional circulation rainfall and hydrological watershed model. Journal of Hydrologic Engineering, 17: 43-54.

Skamarock W. C., Klemp J. B., Dudhia J., Gill D. O., Barker D. M., Duda M. G., Huang X. Y., Wang W., Powers J. G., 2008. A Description of the Advanced Research WRF Version 3. Available at: www.mmm.ucar.edu/wrf/users/docs

Steiner M., Smith J.A., 2000. Reflectivity, Rain Rate, and Kinetic Energy Flux Relationships Based on Raindrop Spectra. Journal of Applied Meteorology, 39: 1923-1940.

Stensrud D.-J., 2007. Parametrization schemes: keys to understanding numerical weather prediction models. Cambridge University Press, Cambridge UK, 459 pp.

Tiedtke M., 1989. A Comprehensive Mass Flux Scheme for Cumulus Parameterization in Large-Scale Models. Monthly Weather Review, 117: 1779-1800.

Turso S., Paolella S., Gabella M., Perona G., 2013. MicroRadarNet: A network of weather micro radars for the identification of local high resolution precipitation patterns. Atmospheric Research, 119: 81-96.

Uijlenhoet R., 2001. Raindrop size distributions and radar reflectivity–rain rate relationships for radar hydrology. Hydrology and Earth System Sciences, 5: 615-627.

Villarini G., Krajewski W. F., 2010. Review of the different sources of uncertainty in single polarization radar-based estimates of rainfall. Surveys in Geophysics., 31: 107-129.

Villarini G., Seo B-C, Serinaldi F., Krajewski W. F., 2014. Spatial and temporal modeling of radar rainfall uncertainties. Atmospheric Research, 135-136: 91-101.

Wang Y., Chandrasekar V., 2010. Quantitative precipitation estimation in the CASA X-band dual-polarization radar network. Journal of Atmospheric and Oceanic Technology, 27: 1665-1676.

Wilks, D. S., 1995. Statistical methods in the atmospheric science. An Introduction, Academic Press, 464 pages.

Yu X., Lee T., 2010. Role of convective parameterization in simulations of a convective band at grey-zone resolutions. Tellus, 62A: 617-632.

Zhang F., Odins A., Nielsen-Gammon J., 2006. Mesoscale predictability of an extreme warm season precipitation event. Weather and Forecasting, 21: 149-166.

Zhang C., Wang Y., Hamilton K., 2011. Improved representation of boundary layer clouds over the Southeast Pacific in ARW-WRF using a modified Tiedtke cumulus parameterization scheme, Monthly Weather Review, 139: 3489-3513.